Feasibility Study of Fast Ion Loss Diagnostics for CFQS by Beam Ion Loss Calculation on Vacuum Vessel

K. Ogawa[a,b], M. Isobe[a,b], R. Seki[a,b], H. Nuga[a], H. Yamaguchi[a,b], S. Sangaroon[a,c], A. Shimizu[a,b], S. Okamura[a], H. Takahashi[a,b], T. Oishi[a,b], S. Kinoshita[a], T. Murase[a], S. Nakagawa[a], H. Tanoue[a], M. Osakabe[a,b], H. F. Liu[d], and Y. Xu[d]

[a] *National Institute for Fusion Science (NIFS), National Institutes of Natural Sciences, 322-6 Oroshi-cho, Toki-city, Gifu 509-5292, Japan*
[b] *The Graduate University for Advanced Studies, SOKENDAI, 322-6 Oroshi-cho, Toki-city, Gifu 509-5292, Japan*
[c] *Mahasarakham University, 20 41 Kham Riang, Kantharawichai District, Maha Sarakham 44150, Thailand*
[d] *Southwest Jiaotong University, Sha Xi Mei Shi Yi Tiao Jie, Jinniu District, Chengdu, Sichuan, China*
E-mail: ogawa.kunihiro@nifs.ac.jp

ABSTRACT: A feasibility study for installing fast-ion loss diagnostics (FILDs) is initiated to understand energetic ion loss process in a quasi-axisymmetric stellarator CFQS. The calculations of beam ion orbit, the guiding center orbit code including the slowing down by bulk plasma in the Boozer coordinates and the collisionless Lorentz orbit code in the Cartesian coordinates, are performed to estimate the toroidal/poloidal distribution of beam ion losses on a vacuum vessel. We observed that loss points on the vacuum vessel are mainly located at the upper side of torus according to gradient magnetic field drift direction. Based on the loss distribution on the vacuum vessel, a possible location of FILD for CFQS is investigated. Although the energy of lost beam ions is ~10 keV, relatively high-energy (> 20 keV) components can be measured on the upper side of the torus in the low-density case. Furthermore, the radial or vertical dependence of beam ion loss flux at candidate movable scintillator-type FILD positions is obtained. A considerable number of particles reach the scintillator-type FILD position. The energy and pitch angle distribution of beam ions reaching the FILD position shows that scintillator-type FILDs can measure co-going transit beam ions with energy of ~25 keV and pitch angle of ~140 degrees and transition beam ions with energy of 10-15 keV and pitch angle of ~80−100 degrees.

KEYWORDS: CFQS; QAS; Energetic ion confinement; Fast ion loss detector; Orbit following model.

Contents

1. Introduction **1**

2. Setups for orbit following calculation **1**

3. Results of the beam ion loss calculation **2**

3.1 Distribution of lost beam ions on the vacuum vessel 2

3.2 Candidate positions of the fast-ion loss detector 5

4. Summary **7**

1. Introduction

The study of fast-ion losses caused by magnetic field ripples and various magnetohydrodynamic (MHD) instabilities plays a key role in understanding the fusion-born alpha particle losses of a fusion reactor. Moreover, the velocity distribution and flux of escaping energetic ions are essential in understanding confinement-loss boundary and energetic ion transport through wave-particle interaction. Fast-ion loss detectors (FILDs) [1], which provide energy, pitch angle, and flux of lost energetic ions, have been commonly used to understand the energetic ion loss in tokamaks [2-9] and stellarator/helical devices [10-14]. Under a joint project of the National Institute for Fusion Science and Southwest Jiaotong University [15], physics [16-20] and engineering design [21-25] of the world's first quasi-axisymmetric stellarator CFQS have been progressed and CFQS is currently in the course of construction. In CFQS, a neutral beam (NB) injector is considered to be installed. Therefore, a study of energetic ion confinement based on experimental results in quasi-axisymmetric stellarator configuration will be possible for the first time. A feasibility study for the installation of FILD is reported herein.

2. Setups for orbit following calculation

CFQS is classified into a quasi-axisymmetric stellarator with a major radius of 1.0 m and a minor radius of 0.25 m, as shown in Fig. 1. The toroidal magnetic field strength is 1.0 T. CFQS will be equipped with a tangential NB injector with injection energy and power of 30 keV and 1 MW, respectively. A previous numerical study of the NB injection angle was reported in Ref.

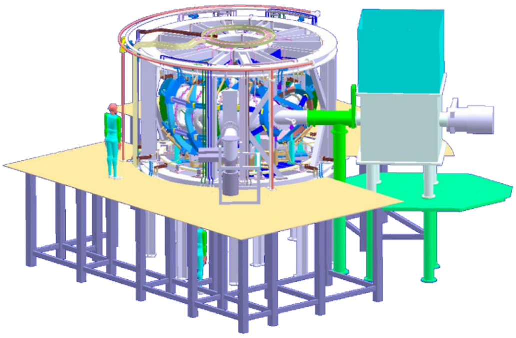

Figure 1. CFQS with NB injector

26. In previous analysis, a hydrogen beam is injected into a hydrogen plasma. Notably the NB direction is counter-aligned with respect to the equilibrium magnetic field. The level of the NB injector axis is located on the equatorial plane of the plasma. This numerical simulation comprises of two parts. One is guiding center orbit calculation based on the birth position of NB, including the slowing down with bulk plasma in the Boozer Coordinates. The other is the collisionless Larmor orbit calculation from the last closed flux surface (LCFS) position where the beam ion reached. The birth position of NB ions is calculated using the HFREYA code, which is a part of the FIT3D code [27], using the three-dimensional MHD equilibrium reconstructed through the VMEC2000 code [28]. Herein, the number of injected particles is set to 5×10^8. The radial profiles of the electron temperature and density are assumed to be parabolic. The central electron temperature (keV) is set to 2.0 / n_{e0} (10^{19} m^{-3}), and the ion temperature is assumed to be the same as the electron temperature. Further, the effective ion charge is 1. The impurity may enhance the pitch angle scattering of beam ions, especially in the relatively low-density/high-temperature case due to the relatively high critical energy. However, in this study, the effective charge is set 1 because the main objectives of this study are to determine whether FILD can work and show the candidate density range. The orbit following calculation, including the finite impurity density based on the experimentally obtained effective ion charge, will be studies in our future work. In this calculation, the central electron density varies from 1×10^{19} to 5×10^{19} m^{-3}. The DELTA5D code [29] is used to calculate the guiding center orbit within 100 ms from the birth position, including the collision with a background plasma in the Boozer coordinates. In the DELTA5D calculation, 10^5 orbits are considered. Note that 10^5 particles are chosen randomly from the deposited particles calculated using the HFERYA code because of the limitation of the computational time. Furthermore, the reaching position and velocity of the energetic ion on the LCFS are obtained. We employ the LORBIT code [30] to calculate the collisionless Lorentz orbit of the NB ion from the LCFS. The orbit following time is set to 0.1 ms, the number of particles is set to 10^6, and the initial position of the collisionless Lorentz orbit is randomly selected from the reaching points on the LCFS calculated using the DELTA5D code with a random number generator. Herein, the gyro phase is also randomly chosen using the random number generator. The number of particles are set to ten times higher than that of DELTA5D code to consider the gyro phase effect. A particle is considered to be lost when the particle reaches the vacuum vessel, whereas the particle is detected by a FILD if the distance between the particle and FILD is less than the Larmor radius. It should be noted that the response of the FILD is not included in this analysis. Therefore, the beam ions coming to the FILD position are considered to be detected. The design of the FILD head will be studied in our future work.

3. Results of the beam ion loss calculation

3.1 Distribution of lost beam ions on the vacuum vessel

A radial distribution of beam ions at different densities is shown in Fig. 2a. The number of source particles corresponding to the deposition efficiency increases with the density in this density region. The integrated number of source particles becomes approximately three times higher in the high-density case (n_{e0} of 5×10^{19} m^{-3}) than the number in the low-density case (n_{e0} of 1×10^{19} m^{-3}). The peak of the number of source particles appeared at the normalized minor radius (r/a) of approximately 0.5-0.6. Moreover, the peak position shifts outward owing to the density increase because the penetration length is short in the high-density cases. Note that the

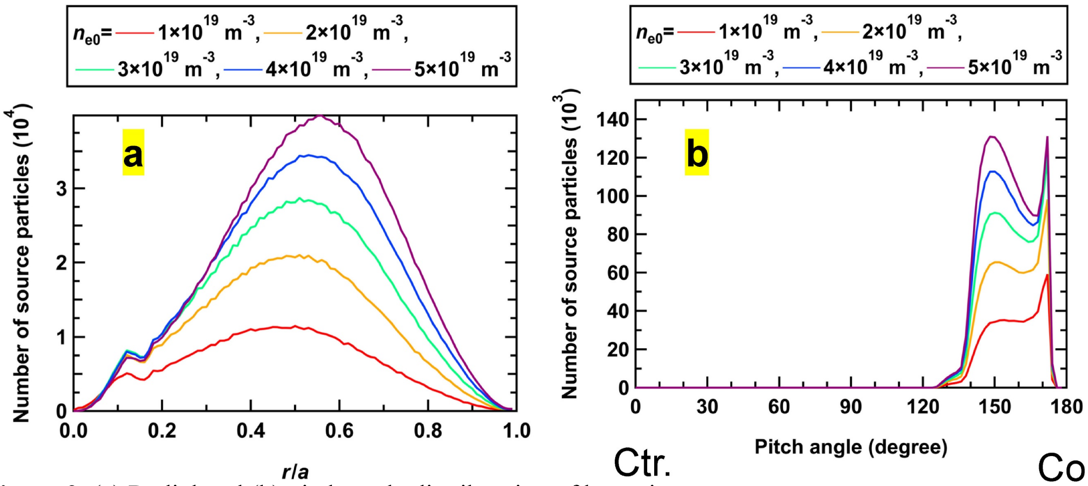

Figure 2. (a) Radial and (b) pitch angle distributuion of beam ions.

number of source particles becomes almost zero at the plasma axis because of the little volume of the plasma. Figure 2b shows the pitch angle distribution of beam ions. The pitch angle of beam ions is mainly greater than 140 degrees, which has co-going passing transit beam ion orbit. A peak at a pitch angle ~150 degrees corresponds to the main components of NB deposition. The other peak at the pitch angle 175 degrees appeared because the tangency point of the plasma axis and the NB sightline exists near the plasma axis as shown in Ref. 19.

Herein, we used the DELTA5D code to obtain the distribution of the reaching points of beam ions with an energy greater than 10 keV on the LCFS (Fig. 3a). In this calculation, the toroidal magnetic field is directed counterclockwise with a topview. Therefore, the reaching points mainly appear at the upper side of the plasma, which is consistent with the gradient magnetic field drift direction. The toroidal and poloidal distribution of the reaching points of beam ions is plotted in Fig. 3b. Here, the size of the toroidal/poloidal angle grid is set to four degrees. In the low-density case, where n_{e0} = 1 × 10^{19} m^{-3}, relatively concentrated regions appear at the toroidal/poloidal angle of 0-40/100-140and 180-220/100-140 degrees. It is worth note that the two preferred toroidal positions appear because of the shape of the equilibrium magnetic field. Thus, the positions are relatively insensitive to the magnetic field strength. However, the positions are relatively sensitive to the equilibrium magnetic field or the magnetic

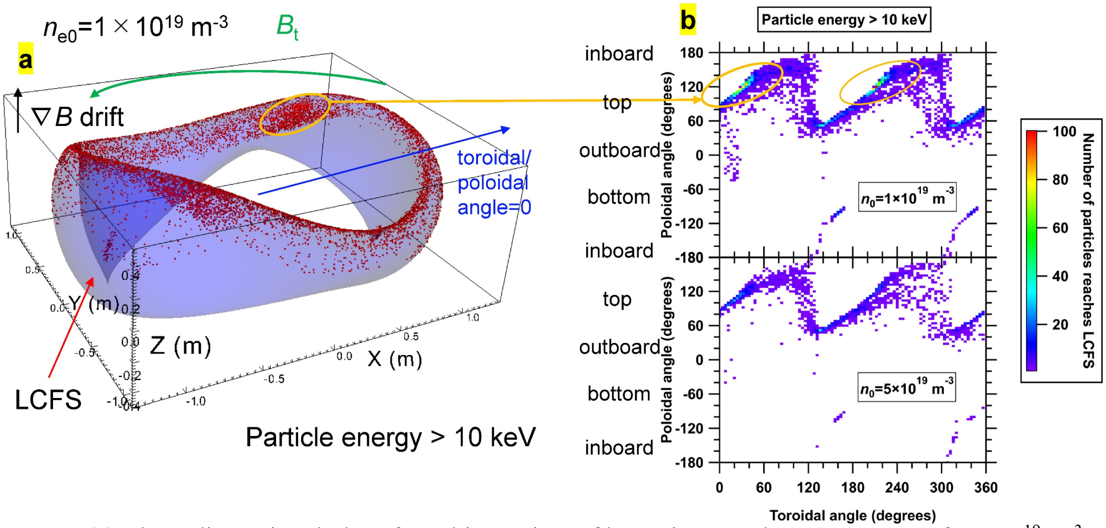

Figure 3. (a) Three dimensional plot of reaching points of beam ions on the LCFS at n_{e0} of 1 × 10^{19} m^{-3}. (b) Toroidal/poloidal angle distribution of beam ion reaching the LCFS.

field direction. The concentrated region corresponds to the relatively high NB heat flux region. Such a concentrated region disappeared in the high-density case, where n_{e0} = 5 × 10^{19} m^{-3}. Figure 4 shows the energy and pitch angle distribution of beam ions reaching the LCFS. For the energy distribution, two sharp peaks appeared at 15 and 30 keV in all density cases, corresponding to the prompt loss of full and half energy components of the NB injector. A relatively broad peak is observed at the energy less than 10 keV. The beam ion reaches the LCFS owing to the orbital effect. The energy decreases as the density increases owing to the shorter slowing down time of beam ions due to a high density and low temperature. For the pitch angle distribution, a relatively significant peak is observed at a pitch angle of 60-110 degrees and relatively small peaks are present at the pitch angle of 130-175 degrees. The former peak corresponds to the thermalized components with energy of less than 10 keV, whereas the latter peak appeares due to the beam ion reaching the LCFS within a short time. The peak at a pitch angle of ~100 degrees might appear at the lowest density case because of the relatively longer slowing down time.

Furthermore, the lost points of beam ions on the vacuum vessel are obtained using the

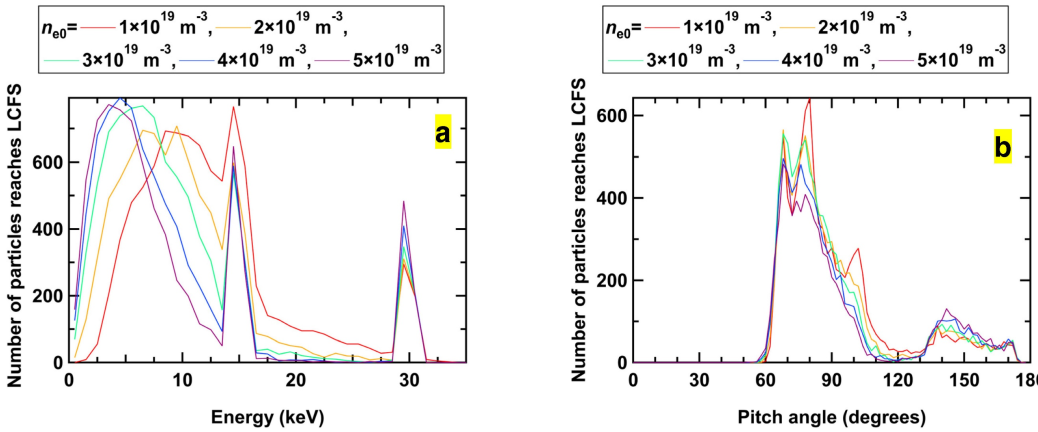

Figure 4. (a) Energy distribution of beam ions reaching the LCFS. (b) Pitch angle distribution of beam ions reaching the LCFS.

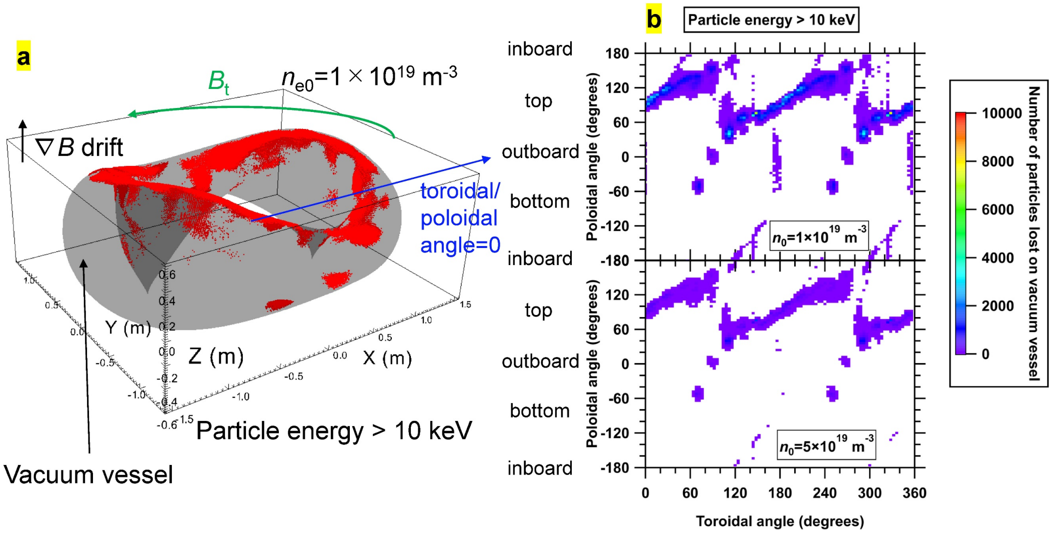

Figure 5. (a) Three dimensional plot of loss points of beam ions on the vacuum vessel at n_{e0} of 1 × 10^{19} m^{-3}. (b) Toroidal/poloidal angle distribution of beam ion loss.

LORBIT code (Fig. 5a). The lost points mainly appear at the upper side of the vacuum vessel because of the gradient magnetic field drift. The distribution of lost particles has a stripe-like distribution as shown in Fig. 5b, which is similar to the distribution of the reaching points of beam ions on the LCFS.

3.2 Candidate positions of the fast-ion loss detector

Regarding the beam ion loss disctibution on the vacuum vessel, we investigate the candidate positions for stacking-foil-type and scintillator-type FILDs. Figure 6 shows the top and three-dimensional views of the candidate location of FILDs. A point at the upper side of the vacuum vessel (x, y, z) = (0.35 m, 0.57 m, and 0.43 m) is selected as the candidate position for the stacking-foil-type FILD, where relatively high beam loss flux is expected (Fig. 7a). Here, the size of the stacking-foil is set to be substantially large, i.e., 10 cm × 10 cm, to obtain

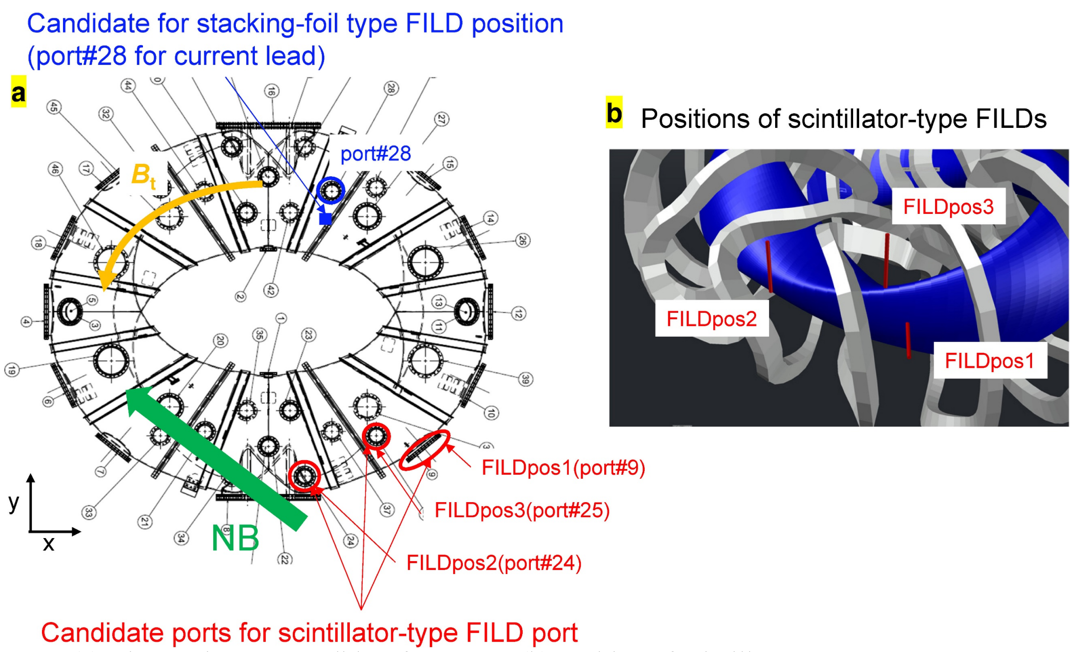

Figure 6. (a) Diagnostics port candidate for FILDs. (b) Position of scintillator-type FILDs.

significant data points in the calculation. Note that port #28 can be used for the current lead

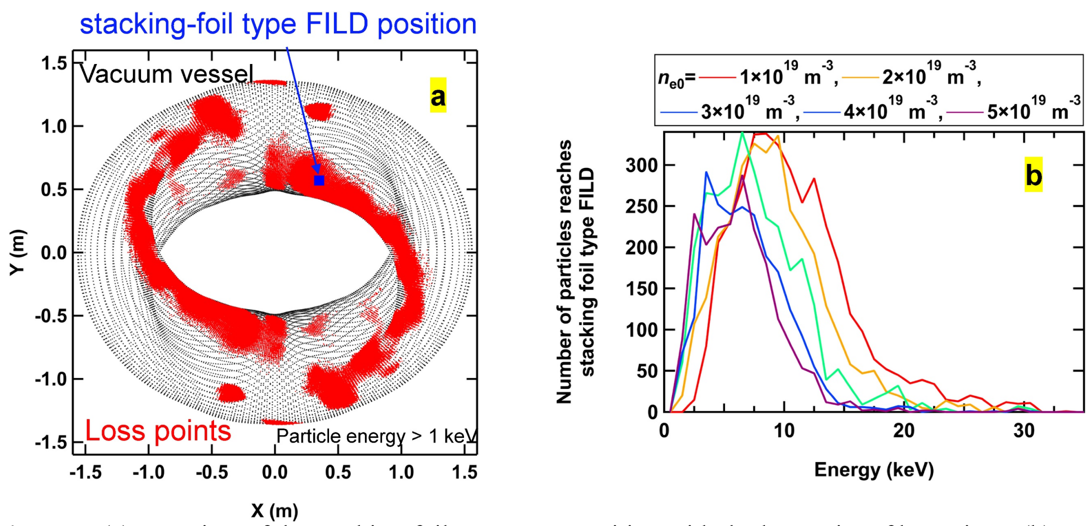

Figure 7. (a) Top view of the stacking-foil type FILD position with the loss point of beam ions. (b) Energy distribution of beam ions reaching the FILD.

connection port. Figure 7b shows that the energy distribution of beam ion reaches the stacking-foil-type FILD position. Some energetic ions having an energy greater than 20 keV can be measured especially in relatively low-density cases (n_{e0} of less than 4×10^{19} m^{-3}). The plot shows that the energy of detectable ions by the stacking-foil-type FILD is mainly less than 10 keV. The relatively low-energy unwanted beam ion flux will be eliminated by the aperture or foil thickness designs.

In Fig. 8, the number of particles detected by the scintillator-type FILD is shown as a function of the position of FILD. In this study, the particle energy greater than 10 keV is counted, and the FILD moves along the FILD axis starting from the diagnostic port. In FILDpos1, the major radius R should be less than 1.3 m to obtain a considerable number of particles (Fig. 8a). The expected signal becomes almost two times higher if the R of the FILD is 1.28 m. However, the density dependence of the number of particles is unclear. In the FILDpos2, height Z should be less than 0.15 m to obtain a considerable number of particles (Fig. 8b). The expected signal becomes almost flat if Z of the FILD becomes less than 0.06 m. The number of particles is higher in relatively low-density cases (n_{e0} of 1×10^{19} and 2×10^{19} m^{-3}). However, the number remains almost unchanged in the higher-density cases. In FILDpos3, the height Z should be less than ~0.31 m to obtain a significant number of particles (Fig. 8c). The expected signal increases with the decrease of Z from 0.31 m to 0.25 m. The number of particles is almost saturated at Z of 0.23 m. The number of particles is higher in relatively low-density cases (n_{e0} of 1×10^{19} and 3×10^{19} m^{-3}). However, the number of particles is almost the same in the high-density cases.

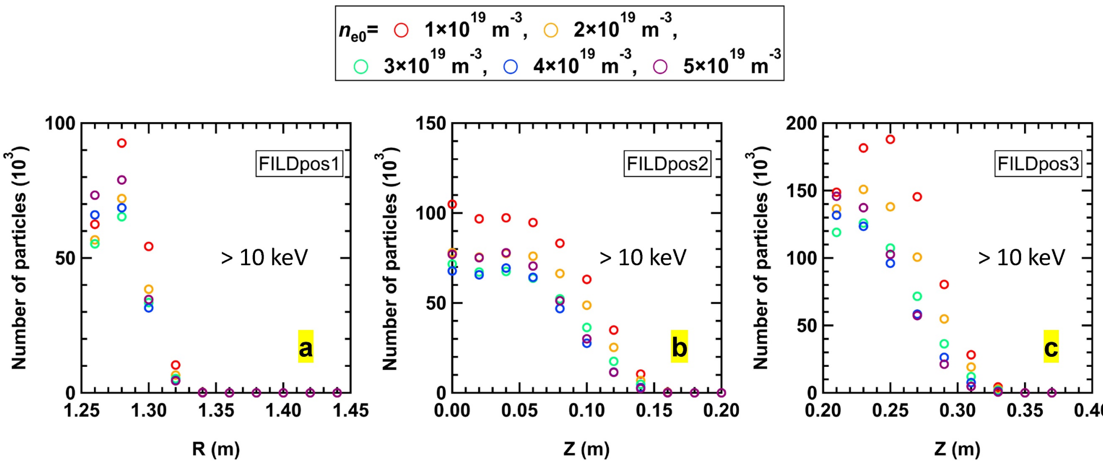

Figure 8. Radial or vertical profile of the number of reaching particles at (a) FILDpos1, (b) FILDpos2, and (c) FILDpos3.

Figure 9 shows the energy and pitch angle distributions of beam ions detected by the FILD at R = 1.28 m for FILDpos1, Z = 0.02 m for FILDpos2, and Z = 0.25 m for FILDpos3. Here, the three spots that exist for energy/pitch angle are ~10 keV/~70 degrees, ~10 keV/100 degrees, and ~25 keV/140 degrees. The former two spots correspond to the barely-trapped ion, whereas the third spot corresponds to the co-going ions near the injection energy. An experimental study of energy/pitch angle resolved toroidal/poloidal distribution of beam ion losses due to magnetic field ripples as well as MHD instabilities becomes prospective for the first time in quasi-axisymmetric stellarator using multiple FILDs.

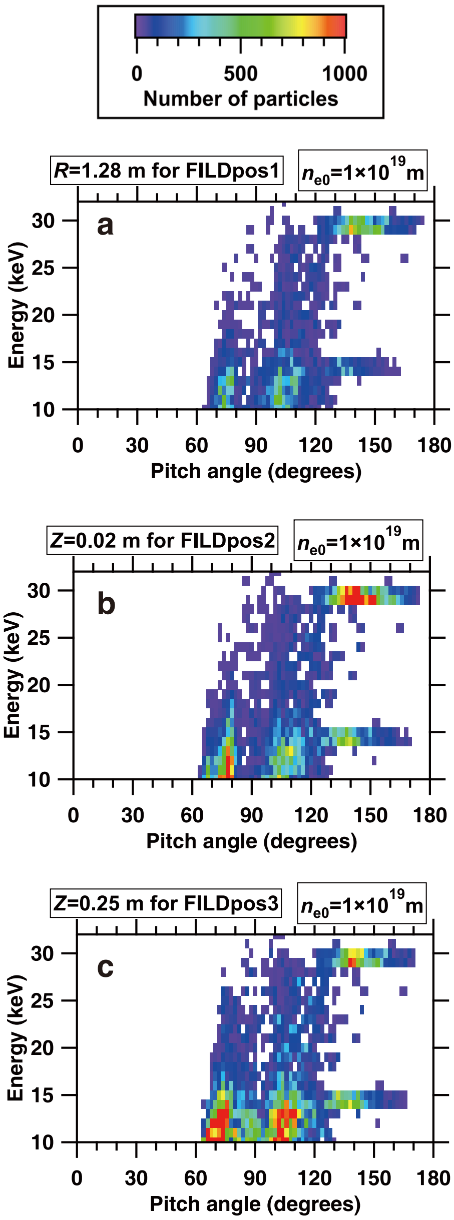

Figure 9. Energy and pitch angle distributions of detectable beam ions by (a) FILDpos1, (b) FILDpos2, and (c) FILDpos3.

4. Summary

CFQS provides the first opportunity for an experimental study of beam ion confinement in a quasi-axisymmetric configuration. A feasibility study of beam ion loss diagnostics was performed using beam ion loss calculation based on the orbit following models. The distribution of beam ion loss on the vacuum vessel shows that the loss points are mainly located at the upper side of the vacuum vessel due to the gradient magnetic field drift. We investigated the candidate positions for FILD and concluded that the measurement of beam ion loss is possible using stacking-foil type and scintillator type FILDs. We hope that the energetic ion confinement study on a quasi-axisymmetric stellarator will be largely progressed using multi-FILDs in CFQS.

Acknowledgments

This work is performed with the support and under the auspices of the NIFS Collaboration Research Program (NIFS17KBAP034). Also, this work is partly supported by International collaborations with overseas laboratories (UFEX105) and Promotion of magnetic confinement research using helical devices in Asia (URSX401).

References

[1] S. J. Zweben, Rev. Sci. Instrum. **60** (1989) 576.

[2] S. Baeumel et al., Fusion Eng Des. **74** (2005) 853.

[3] D. S. Darrow et al., Rev. Sci. Instrum. **72** (2008) 2936.

[4] M. García-Muñoz et al., Rev. Sci. Instrum. **80** (2009) 053503.

[5] D. C. Pave et al., Rev. Sci. Insturm. **83** (2012) 073501.

[6] R. K. Fisher et al., Rev. Sci. Instrum. **81** (2010) 10D307.

[7] Junghee Kim et al., Rev. Sci. Instrum. **83** (2012) 10D305.

[8] Y. P. Zhang et al., Rev. Sci. Instrum. **85** (2014) 053502.

[9] J. F. Chang et al., Rev. Sci. Instrum. **87** (2016) 11E728.

[10] M. Isobe et al., Rev. Sci. Instrum. **70** (1999) 827.

[11] A. Werner et al., Rev. Sci. Instrum. **72** (2001) 780.

[12] S. Yamamoto et al., Rev. Sci. Instrum **87** (2016) 11D818.

[13] K. Ogawa et al., J. Plasma Fusion Res. SERIES **8** (2009) 655

[14] K. Ogawa et al., J. Instrum. **14** (2019) C09021.

[15] M. Isobe et al., Plasma Fusion Res. **14** (2019) 3402074.

[16] H. F. Liu et al., Plasma Fusion Res. **13** (2018) 3405067.

[17] A. Shimizu et al., Plasma Fusion Res. **13** (2018) 3403123.

[18] H. F. Liu et al., Nucl. Fusion **61** (2021) 016014.

[19] J. Varela et al., Nucl. Fusion **61** (2021) 026023.

[20] X. Q. Wang et al., Nucl. Fusion **61** (2021) 036021.

[21] S. Kinoshita et al., Plasma Fusion Res. **14** (2019) 3405097.

[22] A. Shimizu et al., Plasma Fusion Res. **14** (2019) 3403151.

[23] T. Murase et al., Fusion Eng. Des. **161** (2020) 111869.

[24] S. Nakagawa et al., Plasma Fusion Res. **15** (2020) 2405066.

[25] Guozhen Xiong et al., Fusion Eng. Des. **160** (2020) 112021.

[26] K. Ogawa et al., Plasma Fusion Res **14** (2019) 3402067.

[27] S. Murakami et al., Trans. Fusion Technol. **27** (1995) 256.

[28] S. P. Hirshman and O. Betancourt J. Comput. Phys. **96** (1991) 99.

[29] D. A. Spong et al., Phys. Plasmas **18** (2011) 056109.

[30] M. Isobe et al., J. Plasma Fusion Res. SERIES **8** (2009) 330.